THE JOURNAL OF PHYSICAL CHEMISTRY C
A JOURNAL OF THE AMERICAN CHEMICAL SOCIETY

Open Access
This article is licensed under CC-BY-NC-ND 4.0

pubs.acs.org/JPCC
Article

Femtosecond Laser-Induced Emission of Coherent Terahertz Pulses from Ruthenium Thin Films

Lorenzo Cruciani,* Stefan van Vliet, Alessandro Troglia, Roland Bliem, Klaasjan van Druten, and Paul Planken

Cite This: J. Phys. Chem. C 2023, 127, 22662−22672

Read Online
ACCESS | Metrics & More | Article Recommendations | Supporting Information

ABSTRACT: We demonstrate emission of electromagnetic pulses with frequencies in the terahertz (THz) range from ruthenium thin films through a second-order nonlinear optical process. Ruthenium deposited on different substrates showed different THz emission properties. We provide evidence that for Ru on glass above a certain power threshold, laser-induced oxidation occurs, resulting in an increased slope of the linear dependence of the THz electric field amplitude on pump power. The THz electric field is mainly polarized parallel to the sample surface, pointing in the same direction everywhere. In contrast to Ru on glass, the electric field amplitude of the THz pulses emitted by Ru on sapphire and on CaF_2 shows a simple single linear dependence on pump power, and it is polarized orthogonal to the sample surface. In this case, thermal oxidation in an oven enhances the emission and introduces an additional polarization component along the sample surface. This component also points in the same direction everywhere on the surface, similar to the as-deposited Ru on glass. Although the precise THz generation mechanism remains an open question, our results show a strong correlation between the emission strength and the degree of oxidation. Furthermore, the results highlight the importance of the interfaces, i.e., both the choice of the substrate and the chemical composition of the top surface in THz emission experiments. Knowledge of the state of the sample surface is therefore crucial for the interpretation of THz emission experiments from (nonmagnetic) metal surfaces.

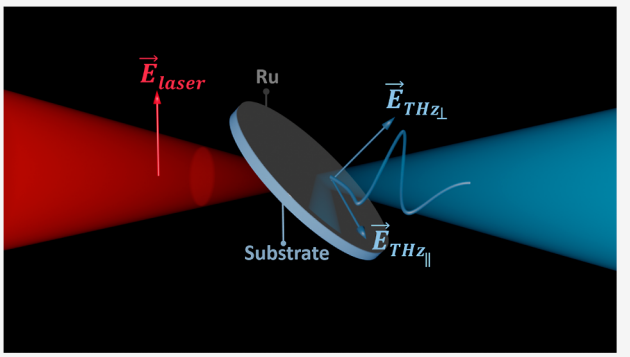

Downloaded via AMOLF on July 8, 2024 at 11:15:47 (UTC).
See https://pubs.acs.org/sharingguidelines for options on how to legitimately share published articles.

INTRODUCTION

Many materials have been shown to emit terahertz (THz) radiation when illuminated with femtosecond laser pulses. The most common ones are semiconductors,[1−3] nonlinear optical crystals such as ZnTe[4,5] and $LiNbO_3$,[6,7] and ferromagnetic metals.[8,9] For these materials, the emission process is typically well understood.

Emission of coherent THz pulses from nonferromagnetic metals has also been demonstrated.[10−12] However, in this case, the generation mechanism is less clear. This is partially caused by several occasionally contradictory observations. For example, high peak fluence illumination of gold gratings was shown to lead to the emission of THz pulses. This was explained by ponderomotive acceleration of photoexcited electrons in the evanescent field of the surface plasmon polaritons (SPPs) excited on the grating, giving rise to a third- to fourth-order dependence of THz power on pump power.[13−15] On the other hand, experiments performed at low peak fluence on Au surfaces also showed SPP-enhanced THz emission,[16] although there, a second-order nonlinear optical process was observed. In this case, unlike in the high laser fluence experiments, the underlying generation mechanism remains an open question.

In general, one of the overlooked aspects in the interpretation of experiments on THz pulse emission from metals is the crucial role that the chemical state and morphology of the sample surface can play. For example, it has been shown that silver can react with H_2S molecules contained in air to create a layer of the semiconductor Ag_2S, forming a Schottky contact with the Ag below. This strongly enhances THz emission through acceleration of photoexcited carriers in the junction's depletion field.[17] Such contamination has been implicated in the search for a possible cause of the difference between THz emission from Au and from Ag observed by Kadlec et al.[10] Still, it remains unexplained how this could cause a change in the order of the nonlinear optical process. Likewise, emission of THz pulses from copper was reported by Suvorov et al.[18] Although recording a surprising exponential dependence of the THz pulse energy on pump

Received: August 16, 2023
Revised: October 12, 2023
Accepted: October 19, 2023
Published: November 9, 2023

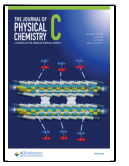

ACS Publications
© 2023 The Authors. Published by American Chemical Society

https://doi.org/10.1021/acs.jpcc.3c05525
J. Phys. Chem. C 2023, 127, 22662−22672

fluence, the state of the sample surface and the possible role of oxidation were not considered. It was subsequently shown, by Ramakrishnan et al.,[19] that oxidation of copper results in the formation of a Cu_2O/Cu Schottky contact, enhancing THz emission. The aforementioned examples indicate that it is crucial to properly determine the state of the sample surface as a starting point for the correct interpretation of the experimental results.

Here, we show that ruthenium thin films also emit THz radiation upon femtosecond laser illumination and that the emission displays a second-order dependence on pump power. Surprisingly, we find that above a certain power threshold illumination of the Ru on glass strongly enhances the emitted THz electric field. This gives rise to a change in the slope of the linear dependence of the THz electric field amplitude on pump power. This process is not observed for films deposited on sapphire and CaF_2, for which a single-slope linear dependence is seen.

Monitoring THz emission before and after annealing of an as-deposited Ru layer in the presence of oxygen and performing X-ray photoelectron spectroscopy (XPS) yield a clear correlation between emission strength and the degree of oxidation. In fact, upon oxidation, we observe an enhancement of the THz emission electric field amplitude by a factor of ∼5.7, corresponding to an increase in the THz power by a factor of ∼33. These results provide strong evidence that the laser-induced enhancement seen above a certain power threshold is, in fact, caused by the partial laser-induced oxidation of the Ru layer.

We also find a surprising dependence of the THz polarization direction on the choice of the substrate. For ruthenium on glass, the THz electric field is parallel to the sample surface and has the same direction everywhere on the surface. For ruthenium on sapphire and on CaF_2, the THz electric field is polarized orthogonal to the sample surface. In this case, thermal oxidation, apart from enhancing the emission, introduces an additional polarization component parallel to the surface, similar to that observed for as-deposited Ru on glass.

Emission is found to be independent of laser polarization direction, suggesting that it is not caused by a coherent laser-induced material polarization but rather by a laser-induced current.

Our results show the importance of the state of the surface in the emission of coherent THz pulses by using femtosecond laser pulses. Moreover, they constitute a potent reminder that the pump laser itself is capable of modifying surfaces, thereby changing the THz emission.

METHODS

The THz generation and detection setup (Figure 1) consist of a Ti/sapphire laser that produces pulses with a central wavelength of 800 nm at a 5.2 MHz repetition rate and a duration of approximately 70 fs. The beam is split into a generation (pump) and a detection (probe) arm. The pump power is varied by means of a half-wave plate and a polarizer and is focused on the sample to a spot with a diameter of about 700 μm. The samples are illuminated from the substrate side, unless otherwise specified. Coherent THz radiation, emitted in the forward direction, is collimated and focused onto a 2 mm thick (110)-ZnTe crystal, where it copropagates with the probe beam. Here, the time-dependent THz electric field is measured through electro-optic sampling.[20] An optical chopper modulates the pump beam at 10 kHz and provides the reference frequency used for lock-in detection. The THz beam path is flushed with dry N_2 gas to minimize absorption from water vapor, reducing the humidity down to $6\%_{RH}$, as measured with a hygrometer.

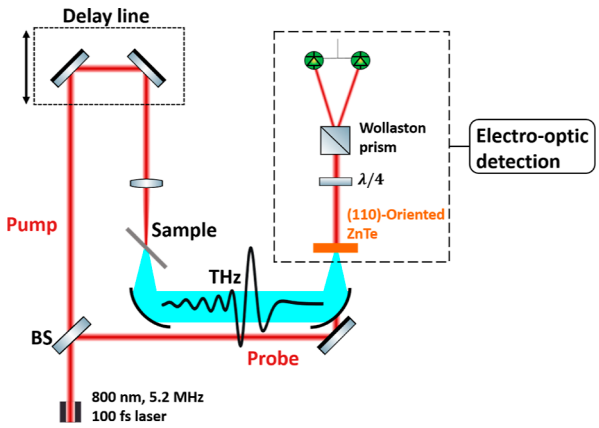

Figure 1. Schematic depiction of the THz generation and detection setup. BS denotes beam-splitter.

Ruthenium thin films were deposited on borosilicate glass and on sapphire and CaF_2 substrates by magnetron sputtering at an argon plasma pressure of 2×10^{-3} mbar, to a thickness of about 8 nm. Before deposition, the glass substrates were chemically cleaned using a solution of ammonium hydroxide (NH_4OH) with hydrogen peroxide and, after that, rinsed in isopropyl alcohol, while the sapphire and CaF_2 substrates were rinsed only in isopropyl alcohol.

THz emission in the forward direction was also observed for Ru layer thickness in a range between 5 and 20 nm without large variations as a function of thickness. Since the 8 nm thick films showed slightly stronger emission than the other thicknesses, most of the results presented below were obtained using 8 nm thick films (unless otherwise noted).

For the XPS measurements, a monochromatic aluminum Kα X-ray source was used (producing 1486.6 eV photons). The number of emitted electrons as a function of their kinetic energy was measured by a Scienta Omicron HiPP-3 analyzer with a 0.8 mm aperture entrance cone and a slit setting of 1.0 mm. The peaks were analyzed using KolXPD software and Doniach-Sunjic peak shapes convoluted with a Gaussian function for ruthenium metal and ruthenium oxide. Voigt peak shapes were used for carbon and ruthenium oxide satellite peaks. A Shirley function was used to subtract the background. More details on the XPS analysis are described in ref 21. The atomic ratios were calculated from the peak areas divided by the respective photoemission cross-section.

Tapping mode AFM images were acquired using a Dimension ICON, Bruker with a RTESPA-300, Antimony (n) doped Si, Bruker tip. The measured images were processed using the Gwyddion software.[22] A fifth-degree polynomial flattening was used to correct the images.

RESULTS

Terahertz Emission and Pump Power Dependence. In Figure 2, we plot the measured THz electric field as a function of time, emitted by an 8 nm thick ruthenium film deposited on glass illuminated at a 45° angle of incidence (AOI). Similar traces have been consistently recorded, showing no significant differences for samples deposited on sapphire and CaF_2. The

https://doi.org/10.1021/acs.jpcc.3c05525
J. Phys. Chem. C 2023, 127, 22662−22672

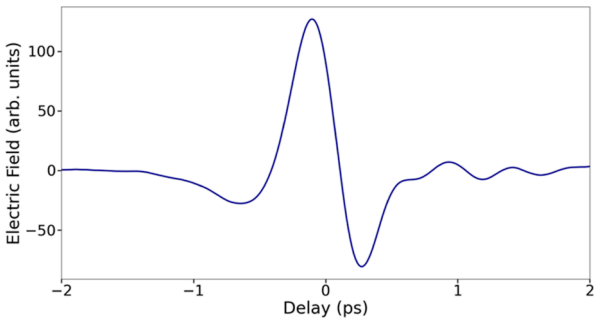

Figure 2. Measured THz electric field as a function of time, emitted from an 8 nm thick Ru layer on glass after illumination with an 800 nm central-wavelength femtosecond laser pulse.

traces consist of single-cycle electric fields from approximately −0.8 to 0.5 ps (relative) delay. The quasi-oscillatory signal seen for delays beyond 0.6 ps is caused by spectral filtering of THz light by water vapor not completely removed by purging with the N_2 gas.[23] We note that the signals typically obtained in our setup from the 8 nm thick Ru samples are rather weak: by a rough comparison, we estimate them to be approximately 3 orders of magnitude lower in amplitude than those obtained from a 0.5 mm (110)-ZnTe crystal.

In order to confirm that the Ru layer is responsible for the THz emission and not the substrate, we also performed measurements on bare substrates. No emission was observed within the sensitivity of our setup. Additionally, measurements on a 150 nm thick Ru layer deposited on glass were also performed by illuminating the samples from the metal side. In this case, no transmission of laser light was detectable, all of it being partially absorbed and partially reflected by the thick metal layer. The penetration depth for 800 nm light in ruthenium is approximately 15 nm.[24] When illuminating the 150 nm thick ruthenium sample from the metal side, no light reaches the Ru/substrate interface. In addition, the electron−phonon coupling constant in Ru is high, so that on the time scale of a few picoseconds, a negligible amount of electron energy reaches the Ru/substrate interface.[25] In this case, THz emission in the reflection direction was also observed but not in the transmission direction. This supports the conclusion that the emission comes from the metal surface (or from a layer near it) rather than from the Ru/substrate interface.

To measure the order of the optical nonlinearity, we extracted the peak-to-peak (pk−pk) field amplitudes of the THz pulses as a function of average pump power, P_{pump}. The resulting curve, measured for 8 nm Ru on sapphire at an AOI of 45°, is plotted in Figure 3. The data follow a linear trend, as highlighted by the linear fit plotted as a solid line. A similar behavior was observed for Ru deposited on CaF_2. These measurements suggest that the emission is due to a second-order nonlinear optical process.

In Figure 4a, we plot the pk−pk field amplitude of the emitted THz pulses as a function of P_{pump} for an 8 nm thick Ru film deposited on glass, illuminated at a 45° AOI. For pump powers below approximately 250 mW (single-pulse pump fluence of 12.5 $\mu J/cm^2$) the THz electric field amplitude scales linearly with pump power. However, around a pump power of 250 mW, a transition to a different linear power-dependence regime is observed, one with a steeper slope extending to at least 700 mW (35 $\mu J/cm^2$). The sudden change in slope at P_{pump} higher than 250 mW deviates from the observations for Ru on sapphire and CaF_2, where no such change was observed.

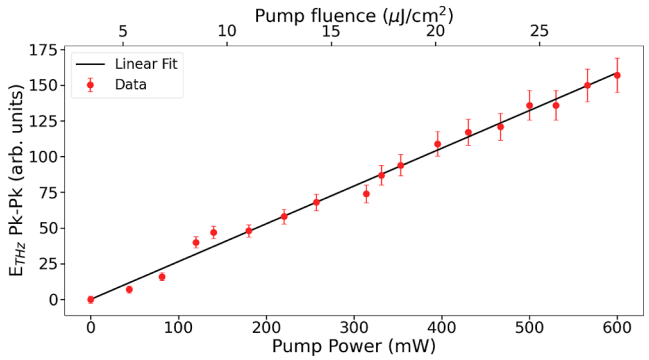

Figure 3. THz pk−pk electric field amplitude as a function of the pump power emitted by an 8 nm thick Ru layer deposited on sapphire. The solid line is a linear fit. Similar results have been obtained for Ru on CaF_2.

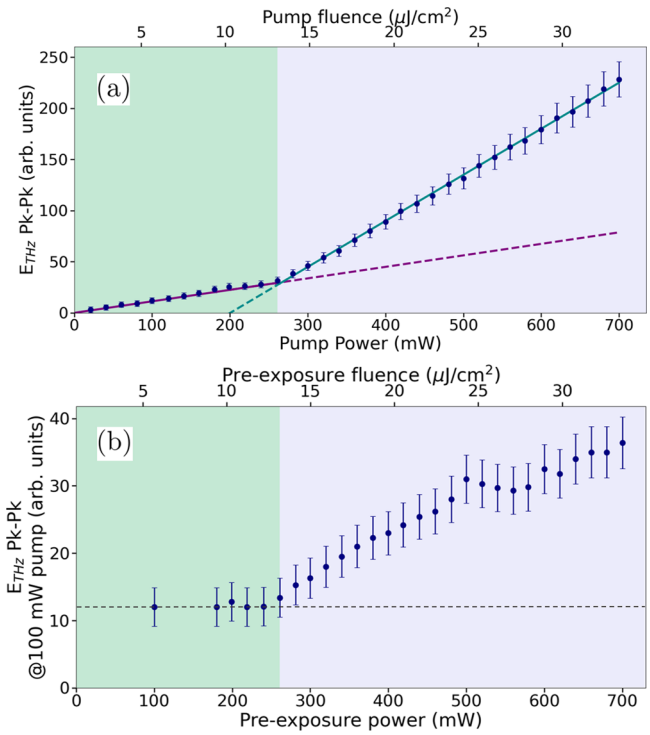

Figure 4. (a) THz peak-to-peak electric field amplitude as a function of pump power for Ru on glass. Linear fits are plotted as solid lines, they are extended as dashed lines to emphasize the different slopes. (b) THz peak-to-peak amplitudes emitted at a fixed reference pump power of 100 mW (pump fluence of 5 $\mu J/cm^2$) as a function of laser pre-exposure power for 240 s exposure time. The horizontal dashed line indicates the THz pk−pk amplitude emitted prior to laser exposure.

As we will show below, the results for Ru on glass are caused by permanent laser-induced material modification occurring at high-power illumination. This modification could be responsible for the enhanced THz emission observed at high power illumination. We point out that the data plotted in Figure 4a were obtained by continuously measuring at the same spot on the sample, going from low to high pump power. This means that each data point is the result of the cumulative exposure to all of the lower powers used previously.

Laser-Induced Material Modifications. The THz emission versus pump power qualitatively changes at a pump

https://doi.org/10.1021/acs.jpcc.3c05525
J. Phys. Chem. C 2023, 127, 22662−22672

power of about 250 mW. Here, we show that these changes are irreversible, indicating a permanent material modification.

In order to monitor the change in THz emission caused by laser exposure, we also recorded the THz emission at a pump power P_{ref} = 100 mW (reference fluence of 5 $\mu J/cm^2$), after pre-exposing the sample to increasing laser powers for a fixed time duration of 240 s. The experiment was carried out by illuminating a single spot and going from low-to-high pre-exposure powers. The peak-to-peak THz electric field emitted by the Ru at a reference pump power of 100 mW (5 $\mu J/cm^2$), as a function of pre-exposure power, are shown in Figure 4b. The data show that the emission amplitude is approximately constant for low exposure powers up to approximately 250 mW (12.5 $\mu J/cm^2$). From 250 to 700 mW (12.5 until 35 $\mu J/cm^2$), the emission amplitude increases, reaching an enhancement factor of THz electric field amplitude of approximately 3, equivalent to a factor of 9 in power. The observed increase of the THz emission at a given pump power after laser exposure is a permanent effect: the metal is permanently modified by laser exposure in a way that makes it capable of emitting more intense THz light. Furthermore, the onset of the "steeper slope" regime in Figure 4a and of the emission enhancement of Figure 4b are both located around 250 mW pump/exposure power (12.5 $\mu J/cm^2$ pump/exposure fluence). This correspondence suggests that the change in the slope of the power dependence is the result of a progressive material modification caused by the pump laser during the measurement.

Thermal Oxidation and X-ray Photoelectron Spectroscopy. Given the results presented above, it seems likely that some form of laser-induced annealing is responsible for the enhanced THz emission observed after high power illumination. We therefore compared THz signals obtained before and after annealing the samples in an oven in a 10^{-3} mbar O_2 atmosphere at 400 °C for 60 min. Before annealing, the samples were kept under vacuum (10^{-5} mbar) for 30 min to allow evaporation of water films on the sample and on the walls of the oven, as well as to purge other contaminants such as carbon-containing molecules.

Figure 5a shows the THz traces obtained before (blue) and after (orange) oxidation of Ru on glass. We observe a THz electric field enhancement factor of approximately 3 after annealing in an O_2 atmosphere. A similar effect is observed for Ru on CaF_2 (Figure 5b) and on sapphire substrates (not shown). The enhancement factor for Ru on CaF_2 is 5.7, which becomes particularly impressive, considering that it corresponds to a 36-fold increase in THz power. The enhanced emission amplitude observed at high pump power from the not-annealed sample seems to be correlated with an increased presence of ruthenium oxide.

Within the signal-to-noise ratio of our experiments and taking the relatively limited phase-matching bandwidth of the 2 mm thick ZnTe detection crystal into account, we are unable to determine whether the rise time or bandwidths of the generated THz pulses before and after oxidation are different.

The same pump-power-dependent measurements as those in Figure 4 were performed on Ru on glass after thermal oxidation at 400 °C in a 10^{-3} mbar oxygen atmosphere for 1 h. Enhanced THz emission amplitude was observed compared with the emission from a pristine sample. However, we recorded a single linear trend with no change in slope at high pump powers, implying that no further laser-induced modification occurs for a sample preoxidized under these conditions.

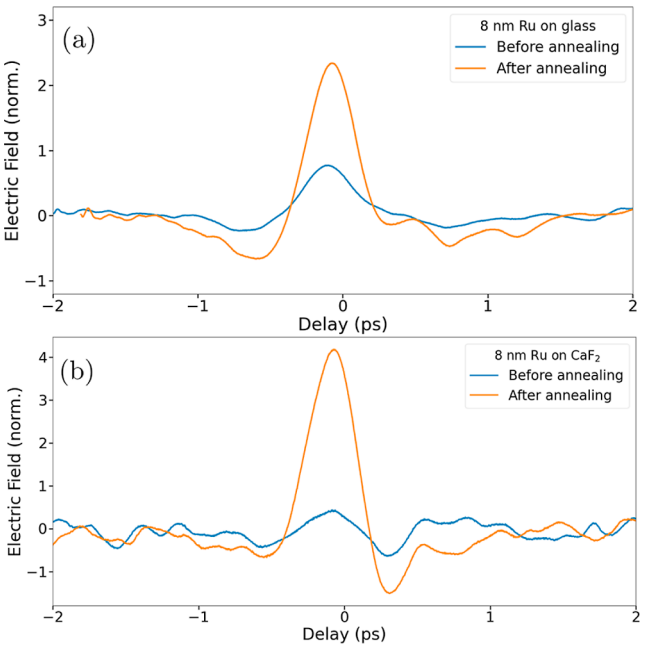

Figure 5. THz electric field as a function of time emitted after excitation with an 800 nm pump pulse measured from 8 nm Ru before (blue) and after (orange) thermal oxidation. The traces are normalized to the peak-to-peak amplitude of the THz pulses obtained before thermal oxidation. (a) Emission from Ru on a glass substrate and (b) emission from Ru on CaF_2.

To confirm the correlation between increased Ru-oxidation and enhanced THz emission, XPS was performed on an 8 nm thick Ru-on-glass sample on an area exposed to high laser power, on an unexposed one and on a thermally oxidized sample.

The resulting data are plotted in Figure 6, showing the Ru 3d lines (Ru $3d_{5/2}$ at 279.8 eV and Ru $3d_{3/2}$ at 284 eV). Figure 6a shows the spectrum of the as-deposited ruthenium (area not exposed to laser light). Apart from the Ru metal peaks, we observe a weak contribution from RuO_x at 281.7 and 286 eV. From these measurements, we calculate a thickness of this oxide layer of approximately 0.5 nm and an atomic ratio of oxidized over metallic ruthenium (RuO_x/Ru-M) of 0.10. We also notice the presence of carbon contamination appearing as the C 1s peak at 284.8 eV. For this sample (pristine Ru, area not exposed to laser light), the atomic ratio of carbon to ruthenium (C/Ru) is 0.32. The XPS spectrum obtained from the area exposed to high laser power is shown in Figure 6b. Relative to the Ru metal peaks, we observe a strong increase of the RuO_x peaks, as well as the rise of the RuO_2 satellite peak at 283.6 eV. The latter is a signature of the presence of the ruthenium oxide rutile phase.[26] In this case, the RuO_x/Ru-M ratio is 1.06. We also observe an increase in the carbon content through the C 1s peak, leading to a C/Ru atomic ratio of 2.16. Compared to the unexposed region discussed previously, this corresponds to a 6.75-fold relative increase in the carbon intensity and a 10-fold increase in the oxidized Ru.

Up to this point, enhanced THz emission resulting from high laser power exposure seems to correlate with both increased ruthenium oxidation and increased presence of carbon. Since we suspected that laser-induced carbon deposition can occur in the ambient atmosphere, we also performed XPS on a sample annealed in a 10^{-3} mbar O_2 atmosphere at 350 °C for 30 min. Similar to the samples used

https://doi.org/10.1021/acs.jpcc.3c05525
J. Phys. Chem. C 2023, 127, 22662−22672

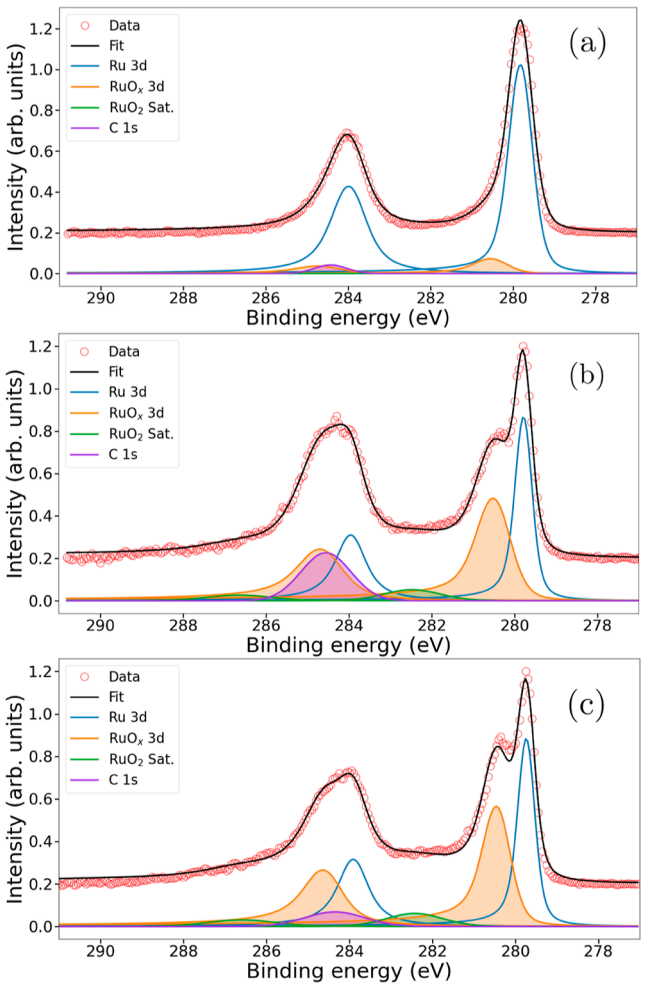

Figure 6. XPS of an 8 nm Ru sample on glass. (a) XPS spectrum measured on a region not exposed to high laser power in air, (b) on a region exposed to high laser power, and (c) on a sample annealed in 10^{-3} mbar of oxygen.

for the measurements reported in Figure 5, these samples were kept under vacuum for 30 min before and after the annealing. We expect this treatment to result in a lower carbon content, allowing to clarify to what extent carbon deposition plays a role in enhancing the THz emission.

Figure 6c shows the resulting XPS spectrum. The spectrum again shows increased ruthenium oxidation, resulting in a RuO_x/Ru-M ratio of 1.03, comparable to the value obtained from the laser-exposed region (1.06, Figure 6b). The C 1s peak located at 284.8 eV, on the other hand, is significantly lower, as can easily be seen by comparing the relative peaks in Figure 6b,c. The resulting C/Ru atomic ratio, in this case, is 0.77.

These results support the conclusion that only increased Ru-oxidation (not carbon deposition) and THz emission strength are strongly correlated.

A qualitative explanation for the fact that the laser-induced THz emission enhancement has not been observed with sapphire, and CaF_2 substrates could be the difference in thermal conductivities between the three substrates. Their thermal conductivities are 1.15 W/(K·m) for glass,[27] 9.7 W/(K·m) for CaF_2[28] and 23 W/(K·m) for sapphire.[29] This implies that the glass substrate allows the metal to retain heat for a longer time after absorption of laser light and to reach a sufficiently high temperature to overcome the reaction barrier for the material modification. The thermal conductivities of the crystalline substrates, on the other hand, could be high enough to cause the Ru temperature to decrease below the value where oxidation can occur more quickly.[30]

It would be interesting to estimate the time evolution of the temperature of Ru during excitation. However, estimating the temperature increase is rather difficult in our case. A maximum Ru temperature shortly after excitation with a single laser pulse can easily be estimated. With a specific heat of Ru of 0.238×10^3 J/(kg·K), an estimated absorbed energy of 29 nJ per pulse, and a laser beam radius on the 8 nm thick sample of about 350 μm, we get a temperature increase for a single laser pulse of about 3.4 K. However, calculating the temperature is significantly more complicated for multiple pulses. This is because we use a 5.2 MHz repetition rate laser. In this case, heat accumulation due to the short time interval between the pulses plays a role, and changes in the absorption coefficient due to gradual heating of the material during excitation are difficult to predict. Furthermore, as we already mentioned, heat diffusion into the substrate is also bound to occur, requiring knowledge about the heat resistivity between the ruthenium and the substrate for an estimate of the temperature reached after a certain time interval. However, our results clearly show that sufficiently high temperatures are reached for a sufficiently long period of time for partial oxidation to occur.

Dependence of THz Emission on the Sample Azimuthal Orientation. Many conventional nonabsorbing THz emitters such as ZnTe or GaP show a distinct azimuthal-angle dependence in the emitted THz polarization direction, when the emitter is rotated around the normal to the surface. As we cannot rule out that our samples might behave in a similar way, we also measured THz emission as a function of the sample azimuthal angle ϕ. This was performed at low pump power (150 mW, 7.5 μJ/cm^2) to avoid self-induced material modifications.

In general, $\vec{E}_{THz}$ can be decomposed into a component parallel, $\vec{E}_{THz\parallel}$, and orthogonal, $\vec{E}_{THz\perp}$, to the sample surface (see inset of Figure 7b). At an AOI of 45°, both the in-plane and orthogonal-to-the-surface electric field have a component perpendicular to the pump and probe beam propagation direction and can therefore be measured in our setup. Changing the azimuthal angle by rotating the sample around the direction normal to the surface has no effect on $\vec{E}_{THz\perp}$ since it is parallel to the rotation axis. This means that the presence of the component of the THz polarization orthogonal to the sample surface results in a ϕ-independent offset in the azimuthal-angle-dependent measurements. A ϕ-dependent contribution occurs only if $\vec{E}_{THz\parallel}$ is present and if it points toward a fixed direction on the sample surface. In this case, rotating the sample rotates this polarization component as well, with respect to the fixed laser polarization.

The THz traces obtained as a function of the azimuthal angle of an 8 nm Ru sample on glass, illuminated at a 45° AOI, are plotted in Figure 7a. The amplitude of the pulses clearly depends on the angle ϕ, and the absolute value reaches a maximum for ϕ = 180, 0, and 360° and reaches a minimum for ϕ = 90 and 270°. The measurements were performed at a fixed orientation of the ZnTe detection crystal. Although we did not determine the absolute sign of E_{THz} with our setup (see the Methods section and a study by Planken et al.[20]), changes in the sign of the THz peaks correspond to actual flips in the sign of the THz electric field.

https://doi.org/10.1021/acs.jpcc.3c05525
J. Phys. Chem. C 2023, 127, 22662−22672

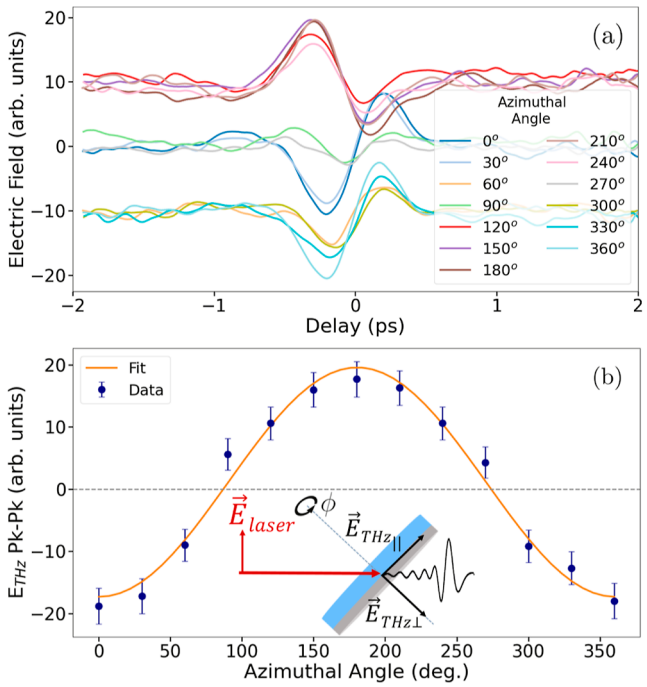

Figure 7. (a) THz traces obtained at different azimuthal orientations at a 45° AOI for Ru deposited on glass. The traces have been vertically displaced in three groups for clarity, despite corresponding to the same set of measurements. (b) pk−pk amplitudes extracted from the traces of figure (a) (blue dots) and the fitted curve (orange). Inset: schematic of the two components of the THz electric field vector. The red arrows represent the laser beam propagation direction and its p-polarized electric field.

The peak-to-peak amplitudes of the traces plotted in Figure 7a were extracted, and a plus or minus sign was assigned to the values obtained for each trace depending on the sign of the first peak. In this way, for instance, the trace corresponding to ϕ = 180° results in a positive pk−pk value, while the one at ϕ = 0° in a negative one. This convention has been used for all of the results discussed below. The values obtained from the traces of Figure 7a are plotted in Figure 7b. The data were fitted with a function of the form $A \sin(\phi + \alpha) + \Delta$; A describes the variation of the THz amplitudes as a function of the azimuthal angle ϕ, and Δ is the azimuthally independent contribution to the THz emission (related to $\vec{E}_{THz}$, see above). α is the phase offset. Figure 7b, together with the values of A = 18.5 and Δ = 1.1, shows that for Ru on glass, the main component of the THz polarization is parallel to the sample surface. This conclusion is further supported by the fact that THz emission was also measured at normal incidence. Furthermore, from such azimuthal-angle dependences, we find that the THz-polarization points toward a fixed direction on the surface, such that sample rotations are accompanied by rotations of the THz polarization. At a given orientation of the ZnTe electro-optic detection crystal, there is an optimal sample orientation which maximizes the detected THz signal.[20]

The azimuthal-angle dependence of the in-plane THz-polarization component follows a simple sine (or cosine) dependence and is a linear polarization.[20] However, knowing the absolute linear direction of the THz polarization is not very useful unless we can somehow connect this to another "directional" feature on the sample surface, which we unfortunately have not been able to do. The rotation of the THz polarization highlighted by Figure 7 should be interpreted as a rotation relative to some preferential direction that we were not able to conclusively identify using the diagnostic tools at our disposal.

It should be pointed out that the measurements were performed by focusing the laser on a spot at a somewhat random distance from the rotation axis of the samples. As a result, a different part on the sample is illuminated at each azimuthal angle. Nevertheless, the same THz signal is obtained at a given ϕ throughout the whole sample. This means that the direction of the emitted THz electric field component parallel to the sample surface is the same over the whole sample. The effect is therefore macroscopic, in contrast to the observation of Zhang et al.[12]

To understand whether this azimuthal-angle dependence results from an anisotropy present in the absorption process or whether it occurs purely at the emission stage, we measured the THz emission as a function of pump-polarization direction. The measurements were performed at normal incidence to eliminate the dependence of the sample reflection on the pump polarization. The results (Supporting Information, Figure S1) do not show any measurable dependence on the incident polarization. In contrast, varying the sample azimuthal angle in the same normal incidence configuration produces a clear sinusoidal dependence, strongly suggesting that the azimuthal-angle-dependence stems purely from the emission process. The results obtained by varying the incident pump polarization make it less likely that a macroscopic single-crystal-like pump-induced, second-order nonlinear optical polarization is responsible for the emission.

2D X-ray diffraction at grazing incidence has been performed on a 20 nm Ru sample after confirming that azimuthal-angle dependence of the THz emission was also present for this sample. The sample thickness was chosen in order to reduce X-ray diffraction contributions from the substrate. The measurements were carried out to determine whether a preferred crystal direction was present in our samples (texturing). No preferential crystal orientation was observed within the measurement accuracy (Figure S2).

Surprisingly, no THz pulse generation and thus no azimuthal angle dependence were observed at normal incidence for ruthenium films deposited on sapphire or CaF_2 substrates, unless the samples were thermally oxidized under conditions such as the ones resulting in Figure 5. These observations show a substantial difference between the emission process in the as-deposited Ru on glass and that on sapphire/CaF_2.

To understand the appearance of azimuthal-angle-dependence in the THz emission for Ru deposited on sapphire, THz emission measurements were performed after annealing the 8 nm Ru samples on sapphire in an O_2 atmosphere at a 10^{-3} mbar pressure, for 30 min. The degree of oxidation was varied by changing the annealing temperature T. The samples were then placed at a 45° AOI to access both electric field polarization components of the emitted $\vec{E}_{THz}$, parallel and perpendicular to the surface. THz time traces as a function of ϕ were recorded, and the pk−pk amplitude values were extracted following the same procedure as the one described for Figure 7. The parameters A and Δ were extracted and divided by the THz peak-to-peak amplitude emitted by each sample before annealing (measured on the same day). This scaling was performed in order to circumvent variations of the THz emission due to slight differences between the samples and/or beam alignment. The results are plotted in Figure 8. The sum of the two scaled parameters, which we define here as

https://doi.org/10.1021/acs.jpcc.3c05525
J. Phys. Chem. C 2023, 127, 22662−22672

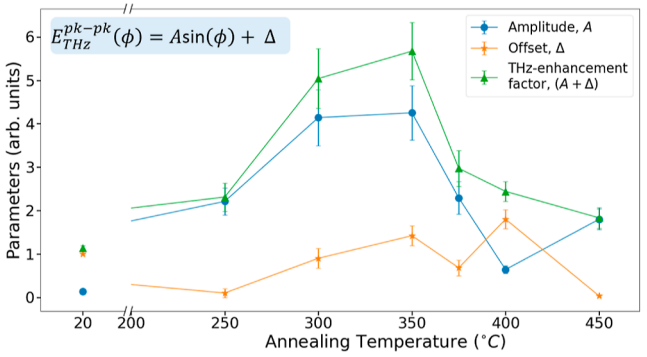

Figure 8. Parameters extracted from azimuthal-angle dependent THz pk−pk amplitude measurements, similar to Figure 7, as a function of annealing temperature for Ru on sapphire. The values are normalized by the azimuthal-angle-independent emission amplitude before thermal oxidation of Ru on sapphire. The parameters were obtained by fitting a function of the form $A\sin(\phi) + \Delta$ to the data. A (blue) is the amplitude of the azimuthal variation, related to the anisotropic component of the THz generation process along the sample surface. Δ is the offset of the sinusoidal curve, related to the component orthogonal to the sample surface. The THz-enhancement factor (green) is the maximum THz electric field obtained as a function of azimuthal angle ϕ.

THz-enhancement factor, shown in green, corresponds to the maximum THz electric field observed as a function of ϕ after annealing, divided by the ϕ-independent THz-peak-to-peak amplitude measured before annealing.

The figure shows that the THz enhancement factor increases with annealing temperatures of up to 350 °C and decreases for higher temperatures. A similar behavior is observed for A and Δ separately, the latter peaking at 400 °C rather than 350 °C.

In agreement with the results of Figure 5, the THz-enhancement factor increases with oxidation. It reaches a maximum value of 5.7 for the electric field, equivalent to a factor of 32 in power, at 350 °C. As explained above, the development of the parameters A and Δ provides information on the direction of the $\vec{E}_{THz}$ vector. Without annealing, the THz field polarization is completely orthogonal to the sample surface for Ru on sapphire and on CaF_2, and thus, no in-plane THz electric field component is present. The growth of the oxide layer introduces a component parallel to the surface, pointing in the same direction everywhere on the sample, as highlighted by the presence of the azimuthal-angle dependence ($A \neq 0$). A increases from 250 °C, peaks at 350 °C, and decreases at higher annealing temperatures; similarly, Δ increases from 250 °C, but it peaks at 400 °C. This seems to indicate that the growth of the oxide layer does correspond to the combined increase of both THz-polarization components, at least until 350 °C annealing temperature.

Surface Morphology: Atomic Force Microscopy. There is a clear azimuthal-angle sine-dependence when the Ru samples are rotated around the surface normal. Normally, this would imply some fixed direction of emission, and one would expect the presence of some form of directionality in the sample, perhaps in the form of oriented microcrystals. For this reason, tapping mode atomic force microscopy (AFM) was used to examine changes in the surface morphology upon thermal oxidation.

Figure 9 shows the results for Ru on glass before (Figure 9a) and after (Figure 9b) thermal oxidation in a 10^{-3} mbar O_2

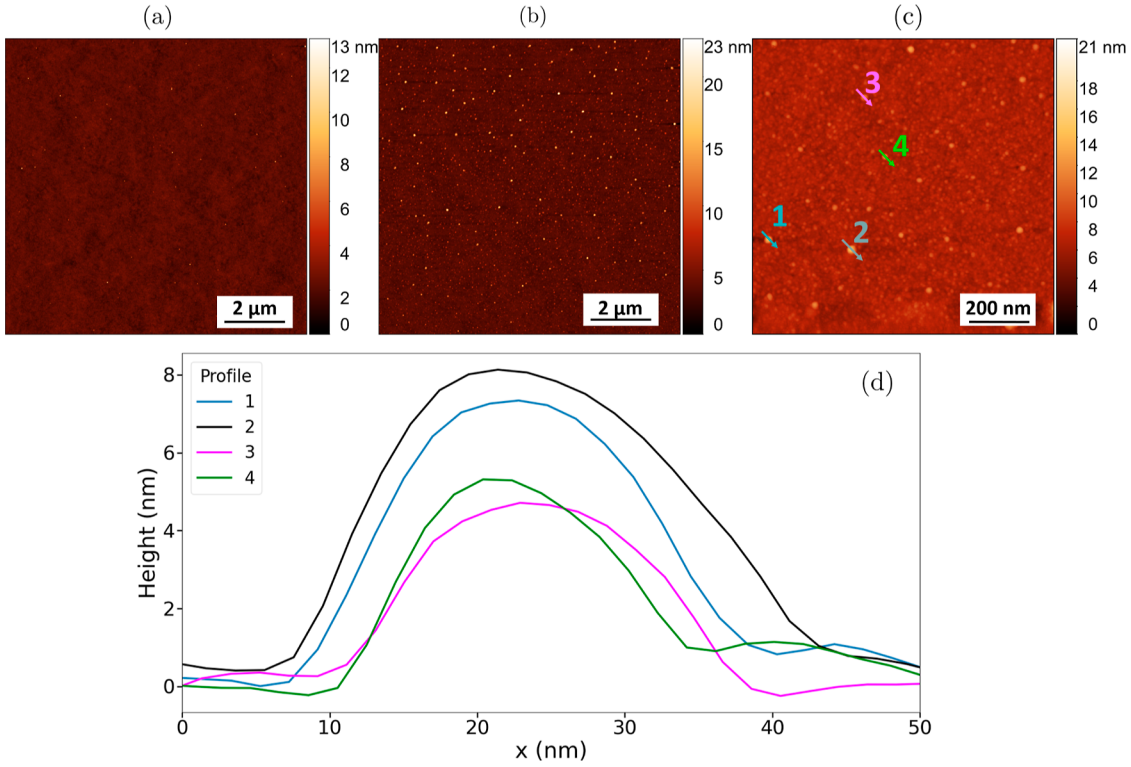

Figure 9. AFM images of Ru on glass (a) before thermal oxidation and (b) after thermal oxidation at 350 °C. Increased presence of nanoprotrusion can be seen by comparing these two images. (c) Zoomed-in AFM image of the thermally oxidized sample. The arrows correspond to the direction of the height cross sections plotted in (d). Here, it can be seen that profile numbers 1, 2, and 4 are steeper on the left side, whereas profile number 3 is symmetric or only weakly asymmetric.

https://doi.org/10.1021/acs.jpcc.3c05525
J. Phys. Chem. C 2023, 127, 22662−22672

atmosphere at 350 °C for 30 min. Increased surface roughness is observed as a result of a higher density of nanoprotrusions (bright spots) on the oxidized sample with respect to the as-deposited one. This observation agrees with the results by Jelenkovic and Tong.[31]

In an attempt to identify the source of the anisotropy observed in the THz emission, we show the AFM image of a smaller area of the annealed sample in Figure 9c. This gives a clearer view of the nanoprotrusions and allows us to extract four height cross sections of these features, indicated in Figure 9c by the numbered arrows and plotted in Figure 9d. Although their size varies, they reach approximately 8 nm in height with a base width of approximately 30 nm. Cross section number 1 shows an asymmetric shape, being somewhat steeper on the left than that on the right. The same applies to profile numbers 2 and 4. The asymmetry is far less evident in profile number 3. We identify these features as the precursors of the nanopillars observed by Coloma Ribera et al. in ref 32.

Although a similar asymmetry appears with different AFM tips and on different samples, we do not exclude the possibility of a tip artifact caused by asymmetric AFM tips.[33] The evidence for the asymmetry is therefore inconclusive.

AFM measurements were also performed on 8 nm Ru deposited on sapphire (Supporting Information, Figures S3). Prior to annealing, we observe a smaller density of the nanoprotrusions compared to Ru on glass. Also, the features are higher in glass compared to sapphire. A similar increase in surface roughness is observed as a function of the annealing temperature. This seems to indicate that such nanoprotrusions might be the source of the anisotropy observed in the THz emission, although proving that this is currently difficult.

DISCUSSION

Correlation between THz-Emission Amplitude and Oxidation. The enhancement of THz emission observed after high-power illumination as well as after annealing in an O_2 atmosphere, in combination with XPS measurements, indicates that oxidation plays an important role in the THz generation process.

Exposing Ru on glass to high laser powers enhances THz emission by a factor of approximately 3 in the THz electric field (9 in THz power, Figure 4a,b) and increases both oxidation and carbon content (Figure 6a) with respect to the as-deposited samples. Annealing of pristine Ru on glass in O_2 results in a similar THz emission-enhancement factor (Figure 5) and oxide content, compared to the previous case, but a much lower increase in the carbon content (Figure 6b). Therefore, the THz emission strength strongly correlates with oxidation. The correlation with the carbon content, if present, is much weaker. As a consequence, it seems likely that oxidation causes the change in the slope of the THz electric field amplitude dependence on pump power for Ru on glass by enhancing the THz emission (Figure 4a,b). This correlation points toward a generation mechanism based on the interaction between the Ru and the Ru-oxide layers.

It has been demonstrated (Figure 6a) that a thin subnanometer thick (~0.5 nm) layer of oxide is formed on top of a ruthenium film under ambient conditions, a feature observed also by Coloma Ribera et al.[32] Thermal annealing has been proven to lead to the formation of the rutile phase RuO_2.[34] Although we are unable to precisely monitor the thickness of the Ru and RuO_2 layers for each annealing temperature, the oxidized layer is known to grow in thickness with annealing temperature and with annealing time.[35] We believe that the relatively weak THz emission of the as-deposited samples, compared to the thermally oxidized ones, is due to the small thickness of the native oxide layer formed by contact with the atmosphere.

From the literature and from our XPS measurements, we know that a native oxide forms on the as-deposited Ru thin films upon contact with ambient air,[32,34] a so-called O−Ru−O trilayer. Thermal annealing above a threshold temperature causes the formation of the RuO_2 rutile phase, which grows with the annealing time and temperature. The fact that a single threshold power is observed for the pump power dependence of THz emission from Ru on glass (Figure 4a) indicates that a Ru/RuO_2 bilayer is forming, rather than a heterojunction with multiple layers. Although both Ru and RuO_2 are conductive (RuO_2 has a resistivity of 76 $\mu\Omega$ cm,[36] compared to the one of Ru being 7.1 $\mu\Omega$ cm[37]), they might form a Schottky junction. In that case, acceleration of photoexcited carriers in the junction's depletion field would be a possible generation mechanism, similar to the one described in ref 19 for Cu/CuO_x. However, in our case, the depletion width would most likely be extremely narrow since both Ru and RuO_2 have high carrier concentrations. This emission mechanism, however, would result in a THz electric field polarized orthogonal to the sample surface, which does not explain the in-plane main THz-polarization component that we observe.

The THz emission-enhancement factor grows with increasing annealing temperature, up to approximately 350 °C (Figure 8), after which it starts to decrease again. It is possible that, at this temperature, some optimal relative thickness of the ruthenium oxide with respect to metallic ruthenium is reached.

THz Polarization Direction: Role of the Substrate. Thermal oxidation of Ru, apart from enhancing the THz emission with each substrate tested, also results in a change in the polarization direction of the THz electric field for Ru on sapphire and CaF_2. On these substrates, $\vec{E}_{THz}$ is orthogonal to the sample surface prior to oxidation (no emission when pump is at normal incidence, no azimuthal-angle dependence); a component parallel to the surface appears after oxidation (emission when pump is at normal incidence, azimuthal-angle dependent emission at 45° incidence). Remarkably, ruthenium on glass emits THz pulses with both polarization components when no thermal oxidation is performed. Any time a parallel component is present, a dependence of the THz electric field amplitude on the sample azimuthal orientation is observed. The fact that azimuthal-angle dependence is observed for the as-deposited Ru on glass, but not on sapphire and CaF_2, shows that the substrate plays a role in the THz emission.

Our observations suggest that the degree of oxidation correlates with the presence of a THz-polarization component parallel to the surface. Although such a polarization component is not present in ruthenium as-deposited on sapphire and CaF_2, it is present also in the as-deposited ruthenium on glass. Nevertheless, it is known that chemical reactions can occur, even at room temperature, between metallic films and silicon substrates.[38] We speculate that perhaps a similar effect could be occurring with glass substrates during ruthenium deposition. If true, then a ruthenium oxide layer forms at the interface with the substrate, in addition to the one formed upon contact with air. Chemical changes at the metal/substrate interface would not easily be detectable through XPS due to its surface sensitivity, which is limited to the uppermost ~6 nm. Crystalline substrates such as sapphire and CaF_2 could be

https://doi.org/10.1021/acs.jpcc.3c05525
J. Phys. Chem. C 2023, 127, 22662−22672

chemically too stable, compared to glass, to react with the metal. Furthermore, CaF_2 contains no oxygen. Therefore, although some process at the interface between the metal and the substrate may be occurring, we have evidence that it corresponds to the formation of an additional oxide layer and, in fact, the high stability of SiO_2 (contained in borosilicate glass) compared to that of ruthenium oxide, in principle, does not favor this process.[32,39] Our confidence in this explanation is therefore fairly low.

Search for a Source of Asymmetry. AFM measurements (Figure 9) showed that oxidation is also accompanied by increased surface roughness, related to the growth of nanoprotrusions. Such features seem to tilt toward a preferential direction, but we cannot exclude the possibility that this is a result of a tip artifact. No other measurable asymmetry was found using various diagnostics techniques. 2D-XRD, in fact, showed that, before annealing, our Ru on glass samples consist of polycrystalline Ru with no clearly measurable preferential crystal orientation (see the Supporting Information).

Potential Explanation Based on Previous Observations. We note that THz emission from ruthenium deposited on porous glass was reported by Zhang et al.[12] Azimuthal-angle-dependent THz emission was also observed in that case. Similar to our results, Zhang et al. did not observe azimuthal-angle dependence for Ru deposited on sapphire substrates. The azimuthal-angle dependence was explained by an anisotropic porous glass structure. Although our samples are different from the nanostructured ones by Zhang's group, it is tempting to compare their results with ours. In particular, it would be interesting to find out whether the anisotropy in THz emission that they observed is caused by the porous nanostructure itself or by a more subtle mechanism, still related to the substrate choice, similar to the one taking place in our non-nanostructured ruthenium films.

THz generation from heterostructures composed of a nonmagnetic metal and single-crystal RuO_2 or IrO_2 has been reported very recently by Zhang et al.[40] The proposed generation mechanism is based on current injection from the nonmagnetic metal into the single-crystal oxide and subsequent deflection induced by its anisotropic conductivity. Although we find it unlikely that a crystal-symmetry-based model could apply to polycrystalline films, a similar mechanism could be occurring in our samples if we could assume a weak, sample-wide net orientation of the RuO_2 crystallites. In that case, electrons excited in the metallic Ru would give rise to a current inside the RuO_2 with an in-plane component and thus THz emission with a field component parallel to the surface.

THz emission with a polarization component parallel to the sample surface and independent of the pump-laser polarization direction was reported by Guzelturk et al. for periodic stripe-domain multiferroic materials.[41] In that work, the THz-polarization direction is related to the direction of the ferroelectric polarization, and the THz emission amplitude is shown to correlate with the density of the domain walls (DWs). However, to the best of our knowledge, ruthenium and ruthenium oxide have not been proven to possess any ferroelectric behavior. Therefore, this seems to be an unlikely explanation for the in-plane polarization component observed in our measurements.

CONCLUSIONS

We have shown that 8 nm thick ruthenium films are capable of emitting coherent THz radiation when illuminated with femtosecond laser pulses through a second-order nonlinear optical process. Laser-induced THz-field enhancement was observed when using glass substrates. This manifests itself as a change in the slope of the linear dependence of the THz-field amplitude on pump power at a certain threshold and as an increased emission at a fixed pump power as a result of pre-exposure to high laser powers. XPS shows that this behavior is most likely due to laser-induced oxidation. The laser-induced enhancement was not observed for films deposited on sapphire or CaF_2. For these samples, a "pure" linear dependence was observed. Nevertheless, for these substrates, annealing the metal films in an O_2 atmosphere at high temperature resulted in increased emission in addition to the formation of a THz field component parallel to the surface. These results show a correlation between the oxidation and enhanced THz emission for all substrates. We observed a large THz-field enhancement, reaching a factor of 6 for Ru on CaF_2, corresponding to a power enhancement by a factor of approximately 36.

Although the exact generation mechanism of THz electromagnetic radiation from ruthenium thin films as a consequence of femtosecond laser illumination remains an open question, we have provided a comprehensive characterization of the emission features. In addition, our results demonstrate the importance of an accurate determination of the state of the sample surface for the correct interpretation of the experimental results.

ASSOCIATED CONTENT

Supporting Information

The Supporting Information is available free of charge at https://pubs.acs.org/doi/10.1021/acs.jpcc.3c05525.

THz emission peak-to-peak amplitude dependence on the azimuthal orientation of the sample compared to its dependence on pump-laser polarization; 2D-XRD diffraction pattern of a 20 nm Ru on glass sample; and AFM images of an 8 nm Ru film on sapphire, as-deposited and thermally oxidized (PDF)

AUTHOR INFORMATION

Corresponding Author

Lorenzo Cruciani − *Advanced Research Center for Nanolithography, 1098 XG Amsterdam, The Netherlands; Van der Waals-Zeeman Institute, Institute of Physics, University of Amsterdam, 1098 XH Amsterdam, The Netherlands;* orcid.org/0009-0004-1570-4286; Email: cruciani@arcnl.nl

Authors

Stefan van Vliet − *Advanced Research Center for Nanolithography, 1098 XG Amsterdam, The Netherlands*

Alessandro Troglia − *Advanced Research Center for Nanolithography, 1098 XG Amsterdam, The Netherlands;* orcid.org/0000-0003-2357-4288

Roland Bliem − *Advanced Research Center for Nanolithography, 1098 XG Amsterdam, The Netherlands; Van der Waals-Zeeman Institute, Institute of Physics, University of Amsterdam, 1098 XH Amsterdam, The Netherlands;* orcid.org/0000-0002-8714-8942

Klaasjan van Druten − *Van der Waals-Zeeman Institute, Institute of Physics, University of Amsterdam, 1098 XH Amsterdam, The Netherlands; Advanced Research Center for Nanolithography, 1098 XG Amsterdam, The Netherlands*
Paul Planken − *Advanced Research Center for Nanolithography, 1098 XG Amsterdam, The Netherlands; Van der Waals-Zeeman Institute, Institute of Physics, University of Amsterdam, 1098 XH Amsterdam, The Netherlands*

Complete contact information is available at: https://pubs.acs.org/10.1021/acs.jpcc.3c05525

Notes

The authors declare no competing financial interest.

■ ACKNOWLEDGMENTS

This work was conducted at the Advanced Research Center for Nanolithography, a public-private partnership between the University of Amsterdam, Vrije Universiteit Amsterdam, The Netherlands Organization for Scientific Research (NWO), and the semiconductor-equipment manufacturer ASML.

■ REFERENCES

(1) Malevich, V. L.; Adomavičius, R.; Krotkus, A. THz emission from semiconductor surfaces. *C. R. Phys.* **2008**, *9*, 130−141.
(2) Côté, D.; Fraser, J. M.; DeCamp, M.; Bucksbaum, P. H.; van Driel, H. M. THz emission from coherently controlled photocurrents in GaAs. *Appl. Phys. Lett.* **1999**, *75*, 3959−3961.
(3) Vainshtein, S.; Kostamovaara, J.; Yuferev, V.; Knap, W.; Fatimy, A.; Diakonova, N. Terahertz Emission from Collapsing Field Domains during Switching of a Gallium Arsenide Bipolar Transistor. *Phys. Rev. Lett.* **2007**, *99*, 176601.
(4) Dakovski, G. L.; Kubera, B.; Shan, J. Localized terahertz generation via optical rectification in ZnTe. *J. Opt. Soc. Am. B* **2005**, *22*, 1667−1670.
(5) Venkatesh, M.; Chaudhary, A. Generation of temporally shaped Terahertz (THz) pulses from Zinc telluride (ZnTe) crystal using tunable femtosecond laser wavelengths. *13th International Conference on Fiber Optics and Photonics*, 2016; p Tu4A.17.
(6) Wu, X.; Carbajo, S.; Ravi, K.; Ahr, F.; Cirmi, G.; Zhou, Y.; Mücke, O. D.; Kärtner, F. X. Terahertz generation in lithium niobate driven by Ti:sapphire laser pulses and its limitations. *Opt. Lett.* **2014**, *39*, 5403−5406.
(7) Kawase, K.; Sato, M.; Taniuchi, T.; Ito, H. Coherent tunable THz-wave generation from LiNbO3 with monolithic grating coupler. *Appl. Phys. Lett.* **1996**, *68*, 2483−2485.
(8) Beaurepaire, E.; Turner, G. M.; Harrel, S. M.; Beard, M. C.; Bigot, J.-Y.; Schmuttenmaer, C. A. Coherent terahertz emission from ferromagnetic films excited by femtosecond laser pulses. *Appl. Phys. Lett.* **2004**, *84*, 3465−3467.
(9) Hilton, D. J.; Averitt, R. D.; Meserole, C. A.; Fisher, G. L.; Funk, D. J.; Thompson, J. D.; Taylor, A. J. Terahertz emission via ultrashort-pulse excitation of magnetic metalfilms. *Opt. Lett.* **2004**, *29*, 1805−1807.
(10) Kadlec, F.; Kužel, P.; Coutaz, J.-L. Optical rectification at metal surfaces. *Opt. Lett.* **2004**, *29*, 2674−2676.
(11) Kadlec, F.; Kužel, P.; Coutaz, J.-L. Study of terahertz radiation generated by optical rectification on thin gold films. *Opt. Lett.* **2005**, *30*, 1402−1404.
(12) Zhang, L.; Buccheri, F.; Zhang, C.; Zhang, X.-C. Terahertz emission from thin metal films with porous nanostructures. *Appl. Phys. Lett.* **2015**, *107*, 071107.
(13) Maier, S. A. *Plasmonics: Fundamentals and Applications*; Springer, 2007; Vol. *1*.
(14) Zawadzka, J.; Jaroszynski, D. A.; Carey, J. J.; Wynne, K. Evanescent-wave acceleration of ultrashort electron pulses. *Appl. Phys. Lett.* **2001**, *79*, 2130−2132.
(15) Welsh, G. H.; Hunt, N. T.; Wynne, K. Terahertz-Pulse Emission Through Laser Excitation of Surface Plasmons in a Metal Grating. *Phys. Rev. Lett.* **2007**, *98*, 026803.
(16) Ramakrishnan, G.; Planken, P. C. M. Percolation-enhanced generation of terahertz pulses by optical rectification on ultrathin gold films. *Opt. Lett.* **2011**, *36*, 2572−2574.
(17) Ramanandan, G. K. P.; Ramakrishnan, G.; Kumar, N.; Adam, A. J. L.; Planken, P. C. M. Emission of terahertz pulses from nanostructured metal surfaces. *J. Phys. D: Appl. Phys.* **2014**, *47*, 374003.
(18) Suvorov, E. V.; Akhmedzhanov, R. A.; Fadeev, D. A.; Ilyakov, I. E.; Mironov, V. A.; Shishkin, B. V. Terahertz emission from a metallic surface induced by a femtosecond optic pulse. *Opt. Lett.* **2012**, *37*, 2520−2522.
(19) Ramakrishnan, G.; Ramanandan, G. K. P.; Adam, A. J. L.; Xu, M.; Kumar, N.; Hendrikx, R. W. A.; Planken, P. C. M. Enhanced terahertz emission by coherent optical absorption in ultrathin semiconductor films on metals. *Opt. Express* **2013**, *21*, 16784−16798.
(20) Planken, P. C. M.; Nienhuys, H.-K.; Bakker, H. J.; Wenckebach, T. Measurement and calculation of the orientation dependence of terahertz pulse detection in ZnTe. *J. Opt. Soc. Am. B* **2001**, *18*, 313−317.
(21) van Vliet, S.; Troglia, A.; Olsson, E.; Bliem, R. Identifying silicides via plasmon loss satellites in photoemission of the Ru-Si system. *Appl. Surf. Sci.* **2023**, *608*, 155139.
(22) Nečas, D.; Klapetek, P. Gwyddion: an open-source software for SPM data analysis. *Open Phys.* **2012**, *10*, 181−188.
(23) van Exter, M.; Fattinger, C.; Grischkowsky, D. Terahertz time-domain spectroscopy of water vapor. *Opt. Lett.* **1989**, *14*, 1128−1130.
(24) Akhmetov, F.; Milov, I.; Semin, S.; Formisano, F.; Medvedev, N.; Sturm, J. M.; Zhakhovsky, V. V.; Makhotkin, I. A.; Kimel, A.; Ackermann, M. Laser-induced electron dynamics and surface modification in ruthenium thin films. *Vacuum* **2023**, *212*, 112045.
(25) Bonn, M.; Denzler, D. N.; Funk, S.; Wolf, M.; Wellershoff, S.-S.; Hohlfeld, J. Ultrafast electron dynamics at metal surfaces: Competition between electron-phonon coupling and hot-electron transport. *Phys. Rev. B: Condens. Matter Mater. Phys.* **2000**, *61*, 1101−1105.
(26) Morgan, D. J. Resolving ruthenium: XPS studies of common ruthenium materials. *Surf. Interface Anal.* **2015**, *47*, 1072−1079.
(27) Assael, M.; Botsios, S.; Gialou, K.; Metaxa, I. Thermal Conductivity of Polymethyl Methacrylate (PMMA) and Borosilicate Crown Glass BK7. *Int. J. Thermophys.* **2005**, *26*, 1595−1605.
(28) Ballard, S. S.; McCarthy, K. A.; Davis, W. C. A Method for Measuring the Thermal Conductivity of Small Samples of Poorly Conducting Materials such as Optical Crystals. *Rev. Sci. Instrum.* **1950**, *21*, 905−907.
(29) McCarthy, K. A.; Ballard, S. S. New Data on the Thermal Conductivity of Optical Crystals. *J. Opt. Soc. Am.* **1951**, *41*, 1062−1063.
(30) Shin, H. J.; Lee, J.-M.; Bae, S.; Kim, W.-H.; Sim, S. Metal-insulator transition and interfacial thermal transport in atomic layer deposited Ru nanofilms characterized by ultrafast terahertz spectroscopy. *Appl. Surf. Sci.* **2021**, *563*, 150184.
(31) Jelenkovic, E. V.; Tong, K. Y. Thermally grown ruthenium oxide thin films. *J. Vac. Sci. Technol., B: Microelectron. Nanometer Struct.–Process., Meas., Phenom.* **2004**, *22*, 2319−2325.
(32) Coloma Ribera, R.; van de Kruijs, R. W. E.; Kokke, S.; Zoethout, E.; Yakshin, A. E.; Bijkerk, F. Surface and sub-surface thermal oxidation of thin ruthenium films. *Appl. Phys. Lett.* **2014**, *105*, 131601.
(33) Shen, J.; Zhang, D.; Zhang, F.-H.; Gan, Y. AFM tip-sample convolution effects for cylinder protrusions. *Appl. Surf. Sci.* **2017**, *422*, 482−491.
(34) Diulus, J. T.; Tobler, B.; Osterwalder, J.; Novotny, Z. Thermal oxidation of Ru(0001) to RuO2(110) studied with ambient pressure

x-ray photoelectron spectroscopy. *J. Phys. D: Appl. Phys.* **2021**, *54*, 244001.
(35) Stilhano Vilas Boas, C. R.; Sturm, J. M.; van den Beld, W. T.; Bijkerk, F. Oxidation kinetics of transition metals exposed to molecular and atomic oxygen. *Materialia* **2021**, *20*, 101203.
(36) Murakami, Y.; Li, J.; Shimoda, T. Highly conductive ruthenium oxide thin films by a low-temperature solution process and green laser annealing. *Mater. Lett.* **2015**, *152*, 121−124.
(37) Yeo, S.; Park, J.-Y.; Lee, S.-J.; Lee, D.-J.; Seo, J. H.; Kim, S.-H. Ruthenium and ruthenium dioxide thin films deposited by atomic layer deposition using a novel zero-valent metalorganic precursor, (ethylbenzene)(1,3-butadiene)Ru(0), and molecular oxygen. *Microelectron. Eng.* **2015**, *137*, 16−22.
(38) Pasquali, L.; Mahne, N.; Montecchi, M.; Mattarello, V.; Nannarone, S. Formation and distribution of compounds at the Ru−Si(001) ultrathin film interface. *J. Appl. Phys.* **2009**, *105*, 044304.
(39) Chatillon, C.; Nuta, I.; Roki, F.-Z.; Fischer, E. Chemical thermodynamics of RuO2(s). *J. Nucl. Mater.* **2018**, *509*, 742−751.
(40) Zhang, S.; Cui, Y.; Wang, S.; Chen, H.; Liu, Y.; Qin, W.; Guan, T.; Tian, C.; Yuan, Z.; Zhou, L.; et al. Nonrelativistic and nonmagnetic terahertz-wave generation via ultrafast current control in anisotropic conductive heterostructures. *Adv. Photonics* **2023**, *5*, 056006.
(41) Guzelturk, B.; Mei, A. B.; Zhang, L.; Tan, L. Z.; Donahue, P.; Singh, A. G.; Schlom, D. G.; Martin, L. W.; Lindenberg, A. M. Light-Induced Currents at Domain Walls in Multiferroic BiFeO3. *Nano Lett.* **2020**, *20*, 145−151.

https://doi.org/10.1021/acs.jpcc.3c05525
J. Phys. Chem. C 2023, 127, 22662−22672